www.cafetinnova.org

Indexed in
Scopus Compendex and Geobase Elsevier,
Geo-Ref Information Services-USA, List B of Scientific Journals, Poland, Directory of Research Journals

ISSN 0974-5904, Volume 09, No. 02

International Journal of Earth Sciences and Engineering

April 2016, P.P.622-631

Investigation on Elastic Plastic Stage of Asymmetric Rectangular CFST Beams with Unequal Wall Thickness

YANG ZHANG[1,2], CHENJIANG YU[1], BING CHEN[3], SHEXU ZHAO[1] AND SIPING LI[1,*]
[1]*Department of Engineering Mechanics, Shanghai Jiao Tong University, Shanghai 200240, PR China*
[2]*School of Civil Engineering, Nanyang Institute of Technology, Nanyang 473004, PR China*
[3]*Department of Civil Engineering, Shanghai Jiao Tong University, Shanghai 200240, PR China*
Email: *lisp_sjtu@sina.com*

Abstract: Asymmetric rectangular CFST beams with unequal wall thickness subjected to pure bending in the elastic plastic stage are investigated in the paper. The variation of the neutral axis in the elastic plastic stage and the condition of the maximum of the ultimate bending moment are given. A case study of ten CFST beams with different cross sections is also carried out. From the theoretical analysis and the case study, it is determined that for an asymmetric cross section, the neutral axis will move and rotate nonlinearly with the plastic development of the cross section, and the translation and rotation of the neutral axis will undergo a fast-slow-fast process.

Keywords: *CFST; asymmetric cross section; neutral axis; ultimate bending moment; elastic plastic stage; bearing capacity*

1. Introduction

Concrete-filled steel tubular (CFST) columns have been widely used in the high-rise buildings nowadays, which have a lot of advantages compared with conventional reinforced concrete and steel tubular columns [1-6]. Circle, square and rectangle CFST columns are commonly used. Circle CFST columns have the best confining effect. However, square and rectangular CFST columns are easier to construct nodes, and have better bending performance than circle CFST columns.

A lot of research achievements on CFST columns have been obtained [7-11]. In general, the wall thickness of steel tubes is uniform, which is beneficial to the processing of steel tubes. The existing studies mainly focus on CFST columns with uniform wall thickness, and there is almost no research on rectangular CFST columns with unequal wall thickness. The uniform wall thickness is not conducive to make full use of materials, and the unequal wall thickness is a good choice for the cross section optimization. The wall thickness of the steel tubes used in the engineering practice may not be completely equal. So it is very necessary to investigate the mechanical properties of asymmetric rectangular CFST columns with unequal wall thickness, which can be easily degenerated into CFST columns with uniform wall thickness.

It is only found that Lu et al. [12] experimental studied the mechanical behavior of the uniaxial symmetric rectangular CFST beams with unequal wall thickness subjected to pure bending, of which the side wall thickness was equal. Three specimens were tested and the ultimate bending strength was compared with the predicted value based on the current design codes. Meanwhile, a FEM model was developed to investigate the effect of the wall thickness ratio of the steel tube on the ultimate bending strength. They concluded that the ultimate flexural strength of the uniaxial symmetric rectangular CFST beam with unequal wall thickness is superior to that of a CFST beam with uniform wall thickness.

The objective of this investigation is threefold: first, to investigate the variation of the neutral axis of asymmetric rectangular CFST beams with unequal wall thickness subjected to pure bending in the elastic plastic stage; second, to study the condition that should be met when the ultimate bending moment of asymmetric rectangular CFST beams with unequal wall thickness subjected to pure bending reaches its maximum; third, to carry out the case study which includes ten CFST beams with different cross sections and compare their bearing capacity.

2. Theoretical analysis of elastic plastic stage:

2.1 Assumptions and constitutive relationships of materials:

The following assumptions are set up in the theoretical study on the elastic plastic stage of asymmetric rectangular CFST beams with unequal wall thickness subjected to pure bending:

① Planar cross section assumption, i.e., the cross section remains plane after deformation.

② Without consideration of the transverse interaction between the steel tube and the concrete core, each point on the cross section is in the uniaxial stress state during the whole loading process.

③ Steel is regarded as an ideal elastic plastic material (shown in Figure 1(a)). Confined concrete in the compression region is assumed to be ideal elastic

plastic, while confined concrete in the tension region is considered to be linear elastic before the tensile strength of confined concrete (f_{ct}) is reached, and beyond the tensile strength it will exit the work (shown in Figure 1(b)). It is also assumed that confined concrete has the same yield strain as steel, which will lead to the following equation:

$$\frac{f_{cc}}{f_{sy}} = \frac{E_c}{E_s} = m \quad (1)$$

Where, E_s, f_{sy}, E_c, and f_{cc} are the elastic modulus of steel, the yield stress of steel, the elastic modulus of confined concrete, and the compressive strength of confined concrete, respectively. m is the ratio coefficient, which is a constant.

④ Tensile stress is assumed to be positive, and compressive stress is assumed to be negative. Bending moment pointing to the positive direction of the coordinate axis is assumed to be positive; conversely, negative.

⑤ As shown in Figure 2, only the asymmetric rectangular CFST beam with unequal wall thickness subjected to pure bending meeting the condition of the neutral axis passing through both the concrete core and the side walls of the steel tube is studied in this paper.

Based on the third assumption, the stress–strain relationship for steel can be expressed as follows:

$$\sigma_s = \begin{cases} f_{sy} & (\varepsilon_s > \varepsilon_{sy}) \\ E_s\varepsilon_s & (\varepsilon_{sy} \geq \varepsilon_s \geq -\varepsilon_{sy}) \\ -f_{sy} & (\varepsilon_s < -\varepsilon_{sy}) \end{cases} \quad (2)$$

in which σ_s, ε_s, and ε_{sy} are the longitudinal steel stress, longitudinal steel strain, and the yield strain, respectively.

$$\varepsilon_{sy} = f_{sy} / E_s \quad (3)$$

The stress–strain relationship for confined concrete can be expressed as below:

$$\sigma_c = \begin{cases} 0 & (\varepsilon_c > \varepsilon_{ct}) \\ E_c\varepsilon_c & (-\varepsilon_{cc} < \varepsilon_c \leq \varepsilon_{ct}) \\ -f_{cc} & (\varepsilon_c \leq -\varepsilon_{cc}) \end{cases} \quad (4)$$

where σ_c, ε_c, ε_{ct} and ε_{cc} are the longitudinal stress of confined concrete, longitudinal strain of confined concrete, the tensile ultimate strain of confined concrete, and the compressive yield strain of confined concrete, respectively.

$$\varepsilon_{ct} = f_{ct} / E_c \quad (5)$$

$$\varepsilon_{cc} = f_{cc} / E_c \quad (6)$$

The tensile strength of confined concrete is expressed as Equation (7), which is much lower than its compressive strength.

$$f_{ct} = 0.6\sqrt{f_{cc}} \quad (7)$$

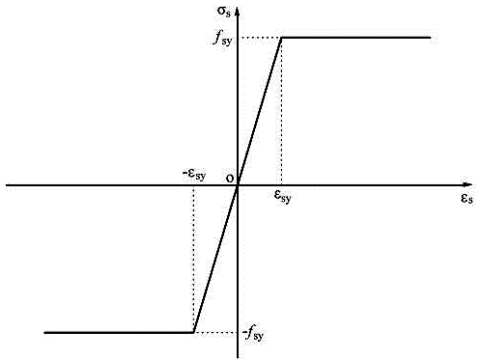

(a) Steel

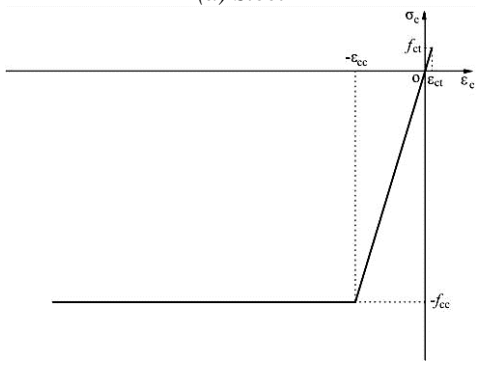

(b) Confined concrete

Figure 1: *Stress–strain curves for steel and confined concrete*

2.2 Bending moment and neutral axis in elastic plastic stage:

The cross section of asymmetric rectangular CFST beams with unequal wall thickness subjected to pure bending in the elastic plastic stage is shown in Figure 2. Based on the fourth assumption, the position of the neutral axis (mn) can be assumed as shown in Figure 2. In order to facilitate the calculation, the whole cross section is divided into thirteen small areas and each area is numbered. The area numbers and the boundaries between the elastic zone and the plastic zone are shown in Figure 2. The coordinate system is also established as shown in Figure 2.

The resultant force ($\overline{N_i}$), and the position vector of the action point of the resultant force ($\overline{r_i}$) on each small area are calculated and shown in Table 1. Based on Table 1 and taking the coordinate origin as the simplified center, the principal vector ($\overline{N}$) and the principal moment vector ($\overline{M}$) of the resultant force of the cross section can be obtained through the following two equations:

$$\overline{N} = \sum_{i=1}^{13} \overline{N_i} = (N, 0, 0) \quad (8)$$

$$\overline{M} = \sum_{i=1}^{13} \overline{r_i} \times \overline{N_i} = (0, M_y, M_z) \quad (9)$$

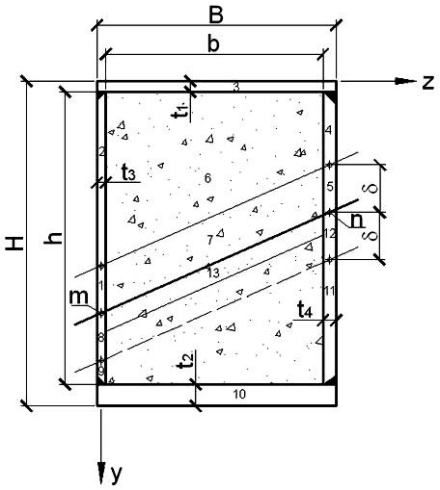

Figure 2: *Cross section of asymmetric rectangular CFST beams*

Due to pure bending, the principal vector must be a zero vector. By solving the equation of $N=0$, the y coordinate of point n (y_n) on the neutral axis can be expressed as below:

$$y_n = \frac{1}{25 f_{sy}(mb+4t_4)}(25 f_{sy}(2b(mt_1-2e_y) + 2H(t_3+t_4)-(4t_3+bm)y_m)+ (9+25mf_{sy})b\delta) \quad (10)$$

in which y_m is the y coordinate of point m on the neutral axis, and δ is half of the width of the steel elastic zone.

The direction angle of the internal bending moment vector (β) can be calculated as follows:

$$\beta = \arctan\frac{M_z}{M_y} \quad (11)$$

The neutral axis vector ($\overline{r_{mn}}$) is expressed as below:

$$\overline{r_{mn}} = (0, y_n - y_m, B - \frac{t_3+t_4}{2}) \quad (12)$$

The direction angle of the neutral axis vector (ϕ) is calculated as follows:

$$\phi = \arctan\frac{B+b}{2(y_n-y_m)} \quad (13)$$

The angle between the internal bending moment vector and the neutral axis vector (γ) is calculated as below:

$$\gamma = \arccos\frac{\overline{M}\cdot\overline{r_{mn}}}{M\ r_{mn}} \quad (14)$$

Where M and r_{mn} are the norms of the vectors of $\overline{M}$ and $\overline{r_{mn}}$. The angles of β, ϕ and γ meet the following equation:

$$\gamma = \phi - \beta \quad (15)$$

Based on Equation (10), all the variables can be expressed as the functions of y_m and δ. The internal bending moment obviously depends on the external bending moment of which the direction is known. So β is determined through the equilibrium equation between the internal and external bending moments, which means that β can be regarded as a constant ($\beta = const$). By solving the equation of $M_z = M_y \tan\beta$, y_m can be expressed as the function of δ. Then all the variables eventually become the functions of δ. Through continuously reducing the value of δ from $h/2$ to zero, a series of the corresponding values of the variables of y_m, y_n, $\overline{M}$, $\overline{r_{mn}}$, ϕ and γ can be obtained. The flow chart of the whole procedure is shown in Figure 3.

2.3 Ultimate bending moment and neutral axis in plastic stage:

The variable of δ represents the plastic development of the cross section. When δ is set to zero, the cross section will become completely plastic, and the bending moment will reach its ultimate bending moment ($\overline{M_u}$). The ultimate bending moment relies on the direction of the external moment, which means that the ultimate bending moment varies with the angle of β. To investigate the maximum of the ultimate bending moment ($M_{u\max}$), the angle of β is no longer regarded as a constant. The program flow chart is shown in Figure 4. As displayed in Figure 4, all the variables of y_n, $\overline{M_u}$, $\overline{r_{mn}}$, ϕ, β and γ can be expressed the functions of y_m. Through continuously increasing the value of y_m from t_1 to $H-t_2$, a series of the corresponding values of the variables of y_n, $\overline{M_u}$, $\overline{r_{mn}}$, ϕ, β and γ can be obtained.

The maximum of the ultimate bending moment can be got by solving the following equation:

$$\frac{dM_u}{dy_m} = 0 \quad (16)$$

Where M_u is the norm of the vector of $\overline{M_u}$. By introducing the solution of Equation (16) into the other variables, the maximum of the ultimate bending moment and its corresponding values of the variables of y_n, $\overline{r_{mn}}$, ϕ, β and γ will be obtained.

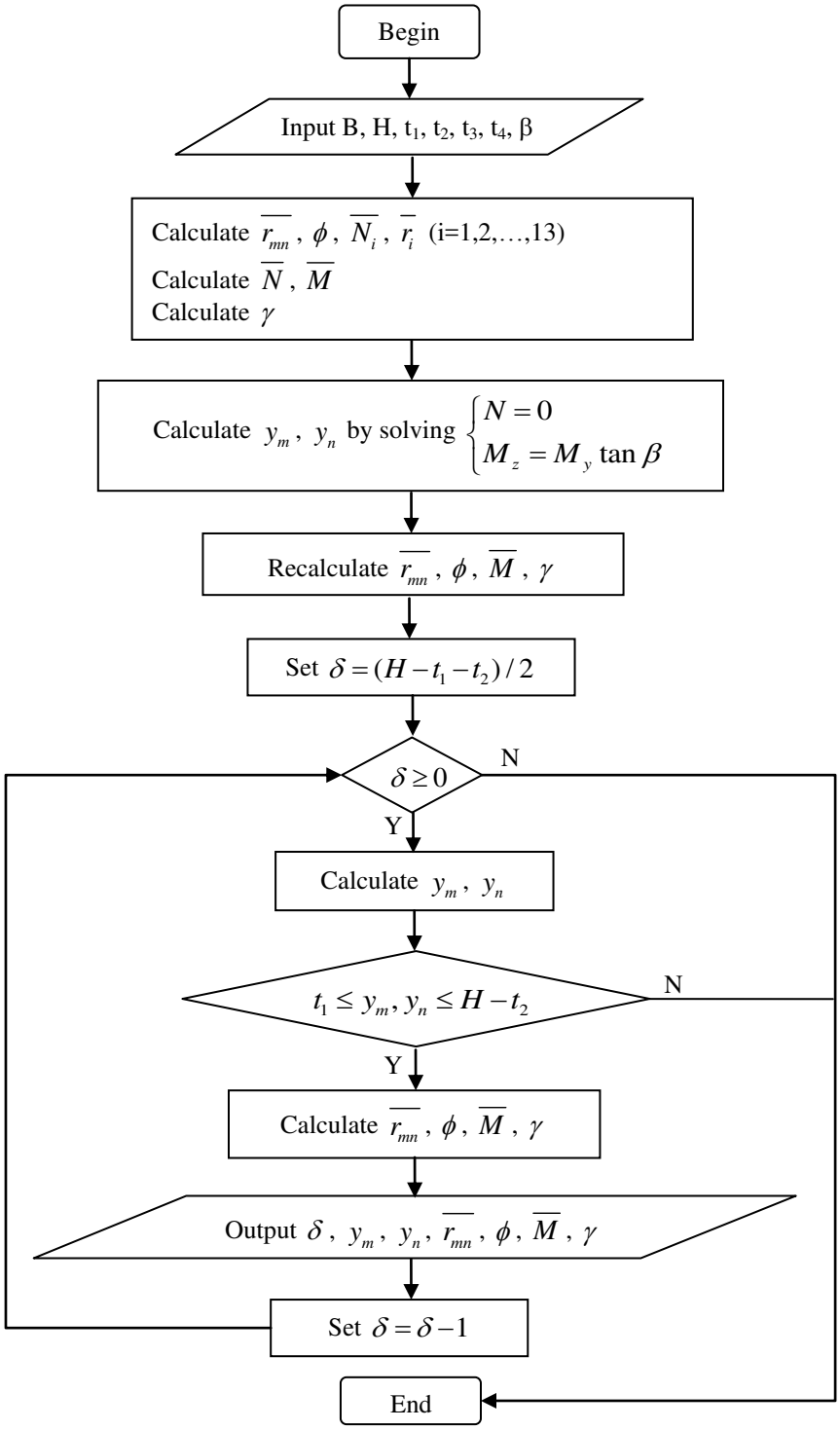

Figure 3: *Program flow chart of elastic plastic stage*

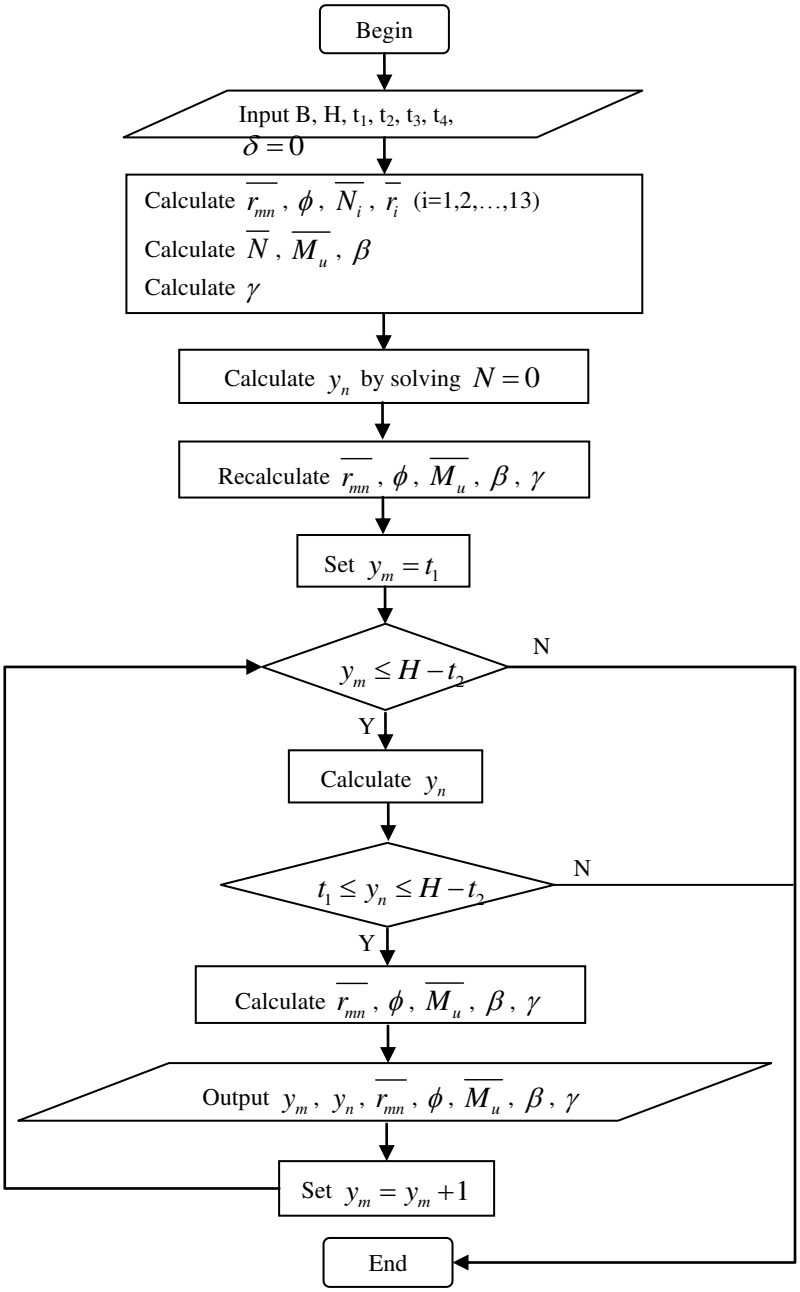

Figure 4: *Program flow chart of plastic stage*

Table 1: *Resultant force and its action point of each sub-area of the cross section*

Area No.	$\overline{N_i}$	$\overline{r_i}$
1	$(-\frac{f_{sy}\delta t_3}{2}, 0, 0)$	$(0, y_m - \frac{2\delta}{3}, 0)$
2	$(-f_{sy}(y_m - \delta - t_1)t_3, 0, 0)$	$(0, \frac{y_m - \delta + t_1}{2}, 0)$
3	$(-f_{sy}Bt_1, 0, 0)$	$(0, \frac{t_1}{2}, \frac{B - t_3}{2})$
4	$(-f_{sy}(y_n - \delta - t_1)t_4, 0, 0)$	$(0, \frac{y_n + t_1 - \delta}{2}, B - \frac{t_3 + t_4}{2})$
5	$(-\frac{f_{sy}\delta t_4}{2}, 0, 0)$	$(0, y_n - \frac{2\delta}{3}, B - \frac{t_3 + t_4}{2})$

6	$(-\frac{1}{2}mf_{sy}b(y_n+y_m-2\delta-2t_1),0,0)$	$(0,\frac{3t_1^2-y_m^2-y_my_n-y_n^2+3\delta(y_m+y_n-\delta)}{6t_1-3(y_m+y_n-2\delta)},$ $b+\frac{t_3}{2}-\frac{b(3t_1-2y_m-y_n+3\delta)}{6t_1-3(y_m+y_n-2\delta)})$
7	$(-\frac{mf_{sy}\delta b}{2},0,0)$	$(0,\frac{y_m+y_n}{2}-\frac{2\delta}{3},\frac{B-t_4}{2})$
8	$(\frac{f_{sy}\delta t_3}{2},0,0)$	$(0,y_m+\frac{2\delta}{3},0)$
9	$(f_{sy}(H-y_m-\delta-t_2)t_3,0,0)$	$(0,\frac{H+y_m+\delta-t_2}{2},0)$
10	$(f_{sy}Bt_2,0,0)$	$(0,H-\frac{t_2}{2},\frac{B-t_3}{2})$
11	$(f_{sy}(H-y_n-\delta-t_2)t_4,0,0)$	$(0,\frac{H+y_n+\delta-t_2}{2},B-\frac{t_3+t_4}{2})$
12	$(\frac{f_{sy}\delta t_4}{2},0,0)$	$(0,y_n+\frac{2\delta}{3},B-\frac{t_3+t_4}{2})$
13	$(\frac{9}{50}\delta b,0,0)$	$(0,\frac{y_m+y_n}{2}+\frac{2\delta}{5\sqrt{mf_{sy}}},\frac{B-t_4}{2})$

3. Case study:

3.1 Details of CFST beams:

Because the formula is too complicated, the specific analytical formula cannot be obtained. In order to intuitively investigate the variation of the neutral axis in the elastic plastic stage, and the condition that should be met when the ultimate bending moment reaches its maximum, case study is carried out.

As listed in Table 2, ten CFST beams with different cross sections are studied, which can be divided into five types of cross section as shown in Figure 5. Each type of cross section consists of the rectangular cross section (R) and the square cross section (S). Section 1 and 2 are asymmetric cross sections, while section 3, 4 and 5 are uniaxial or biaxial symmetric cross sections. The z direction of section 3, 4 and 5 about the middle position of the cross section is symmetric. All the ten specimens have the same steel ratio (α_{sc}) of 0.29.

Table 2: *Details of CFST specimens*

Section No.	B /mm	H /mm	t_1 /mm	t_2 /mm	t_3 /mm	t_4 /mm	α_{sc}	$M_{u\max}$ /kNm	β /°	ϕ /°
1 R	110.0	150.0	6.0	12.0	3.0	10.0	0.29	54.4	-86.4	93.6
1 S	128.4	128.4	6.0	12.0	3.0	9.5	0.29	48.5	-85.3	94.6
2 R	110.0	150.0	3.1	12.0	3.1	12.0	0.29	53.1	-87.5	92.5
2 S	128.4	128.4	3.3	12.0	3.3	12.0	0.29	47.2	-87.3	92.7
3 R	110.0	150.0	8.9	18.0	3.0	3.0	0.29	61.2	-90.0	90.0
3 S	128.4	128.4	7.9	16.0	3.0	3.0	0.29	53.0	-90.0	90.0
4 R	110.0	150.0	13.5	13.5	3.0	3.0	0.29	56.1	-90.0	90.0
4 S	128.4	128.4	11.9	11.9	3.0	3.0	0.29	48.1	-90.0	90.0
5 R	110.0	150.0	7.5	7.5	7.5	7.5	0.29	49.3	-90.0	90.0
5 S	128.4	128.4	7.6	7.6	7.6	7.6	0.29	43.6	-90.0	90.0

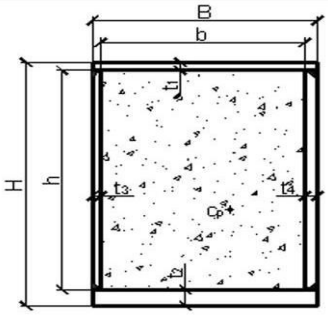

(a) *Section 1*
$t_1 \neq t_2 \neq t_3 \neq t_4$
Asymmetric

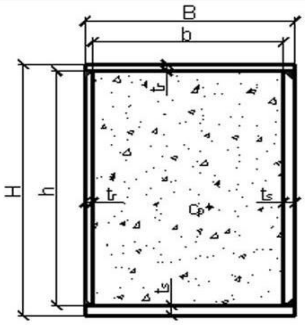

(b) *Section 2*
$(t_1 = t_3 = t_r) \neq (t_2 = t_4 = t_s)$
Asymmetric

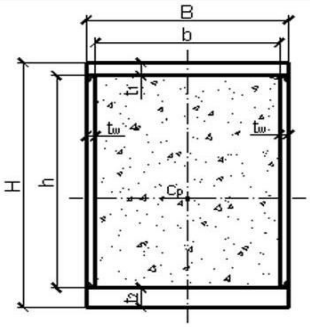

(c) *Section 3*
$(t_3 = t_4 = t_w) \neq t_1 \neq t_2$
Uniaxial symmetric

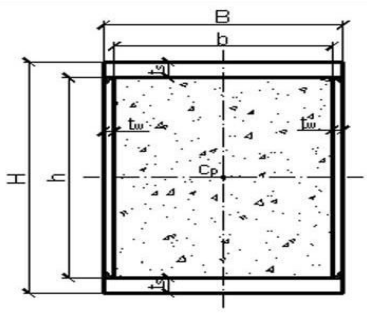

(d) Section 4

$(t_1 = t_2 = t_s) \neq (t_3 = t_4 = t_w)$ *Biaxial symmetric*

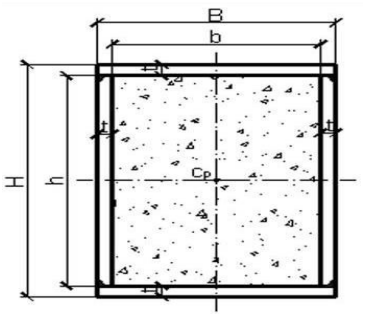

(e) Section 5

$t_1 = t_2 = t_3 = t_4 = t$ *Biaxial symmetric*

Figure 5: *Cross section types*

3.2 Maximum of ultimate bending moment in plastic stage:

A program is compiled based on the program flow chart shown in Figure 4, and a series of the ultimate bending moment and its corresponding values of the variables of y_m, y_n, $\overline{r_{mn}}$, ϕ, β and γ of the ten specimens are calculated. The relationship of ultimate bending moment vs. angle between the ultimate bending moment and the neutral axis of each specimen is shown in Figure 6. It can be seen that the maximum bending moment is achieved when the angle of γ is equal to π, which means that if the ultimate bending moment is collinear with the neutral axis, the ultimate bending moment will reach its maximum. For such asymmetric cross sections as section 1 and section 2, the curves of M_u-γ are also asymmetric (seen from Figures 6(a) and 6(b)). Due to the symmetry of section 3, 4 and 5, their M_u-γ curves are symmetric and the line of $\gamma = \pi$ is the axis of symmetry (seen from Figures 6(c), 6(d) and 6(e)).

The relationship of ultimate bending moment vs. direction angle of the neutral axis of each specimen is shown in Figure 7. It can be seen that, except for section 1 and 2, the curves of M_u-ϕ of the other sections are symmetric about the line of $\phi = \pi/2$. The maximum of the ultimate bending moment, its direction, and the direction of the neutral axis corresponding to $M_{u\max}$ are listed in Table 2. It can be found that, for specimen 1R, 1S, 2R and 2S, the maximum of the ultimate bending moment will be achieved when the direction angles of the neutral axis are 93.6^o, 94.6^o, 92.5^o and 92.7^o, respectively.

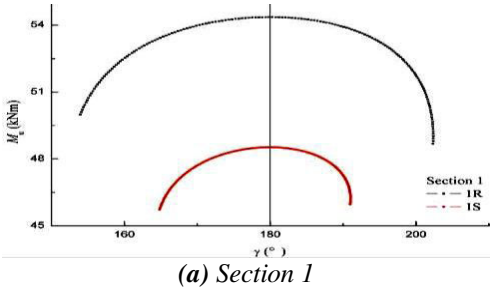

(a) Section 1

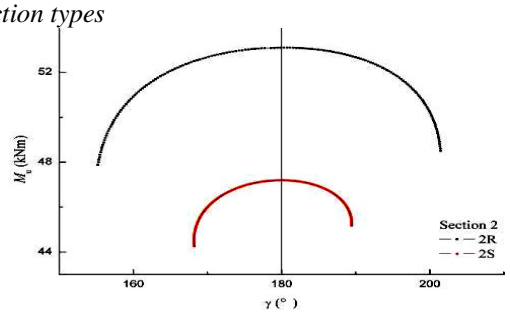

(b) Section 2

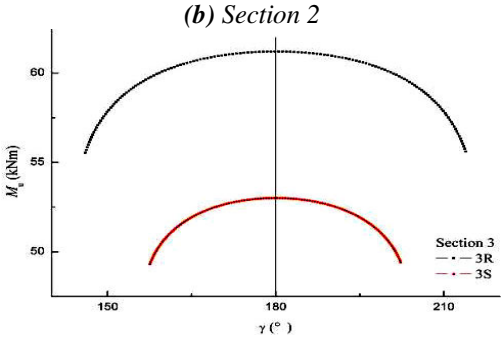

(c) Section 3

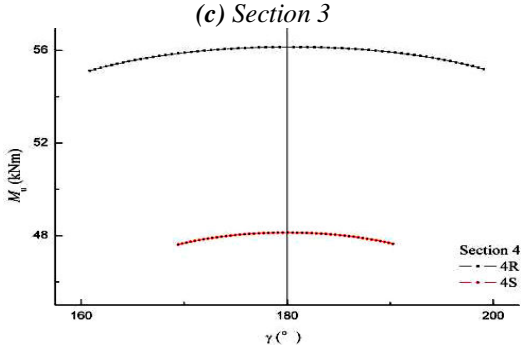

(d) Section 4

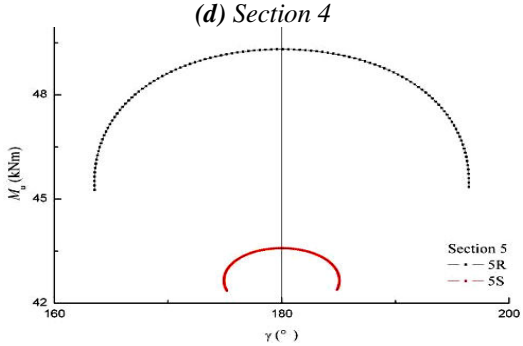

(e) Section 5

Figure 6: *Relationship of ultimate bending moment vs. angle between the ultimate bending moment and the neutral axis*

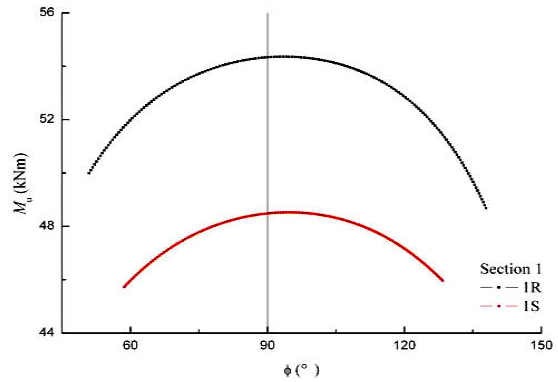

(a) Section 1

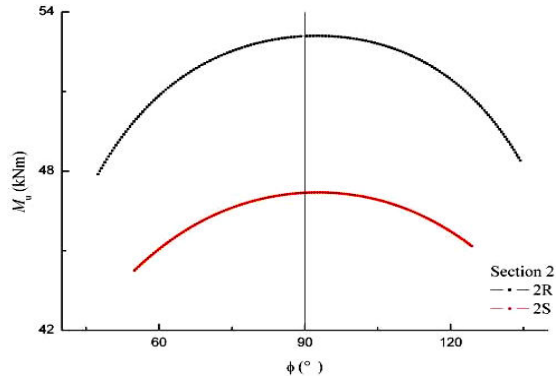

(b) Section 2

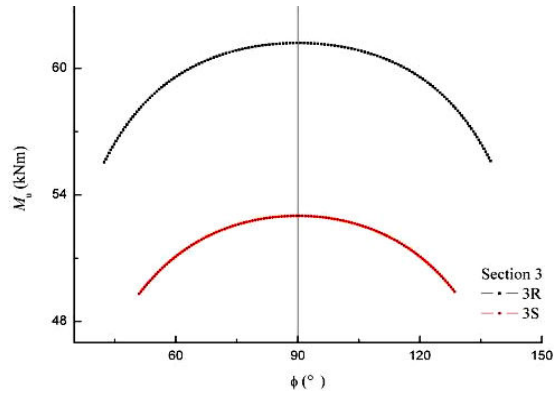

(c) Section 3

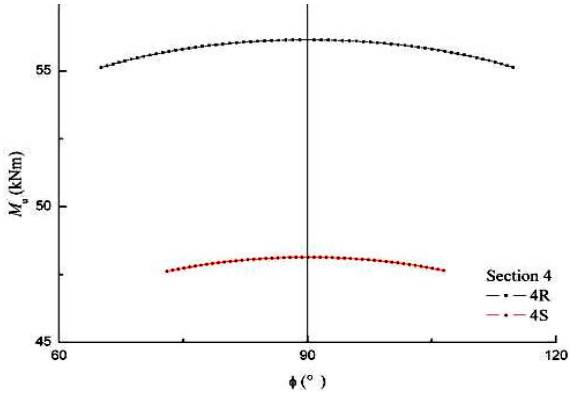

(d) Section 4

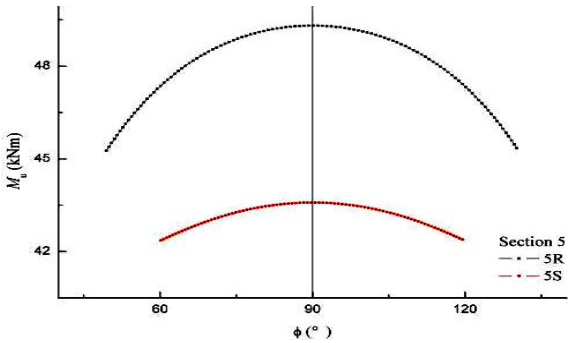

(e) Section 5

Figure 7: *Relationship of ultimate bending moment vs. direction angle of the neutral axis*

3.3 Neutral axis and bending moment in elastic plastic stage:

A program is compiled based on the program flow chart shown in Figure 3, and β is set to the value listed in Table 2 for each specimen, which is the value corresponding to the maximum of the ultimate bending moment. A series of the bending moment and its corresponding values of the variables of δ, y_m, y_n, $\overline{r_{mn}}$, ϕ and γ of the ten specimens are calculated. The position and direction of the neutral axis can be completely determined by the variables of y_m and ϕ. The relationship of direction angle of the neutral axis vs. half of the width of the steel elastic zone of each specimen is shown in Figure 8. It can be seen that, for an asymmetric cross section, the direction angle of the neutral axis in the elastic plastic stage is not a constant, which means that the neutral axis will rotate nonlinearly with the plastic development of the cross section (seen from Figures 8(a), 8(b), 8(c) and 8(d)). It can also be seen that with the varying of δ, the rotation of the neutral axis undergoes a fast-slow-fast process. For specimen 1R, 1S, 2R and 2S, the rotation angles of the neutral axis with δ from $h/2$ to zero are 6.5^o, 4.8^o, 7.7^o and 5.6^o. For such symmetric cross sections as section 3,4 and 5, the direction angle of the neutral axis in the elastic plastic stage remain unchanged as a constant of $\pi/2$, which means that the neutral axis will not rotate with the plastic development of the cross section (seen from Figure 8(e)).

The relationship of y coordinate of point m on the neutral axis vs. half of the width of the steel elastic zone of each specimen is shown in Figure 9. It can be seen that, for an asymmetric cross section, the translation of the neutral axis in the elastic plastic stage with the plastic development of the cross section is approximately linear, but nonlinear in fact (seen from Figure 9(a)). The translation of the neutral axis with δ also undergoes a fast-slow-fast process. For such symmetric cross sections as section 3,4 and 5, the translation of the neutral axis in the elastic plastic stage is absolutely linear (seen from Figure 9(b)).

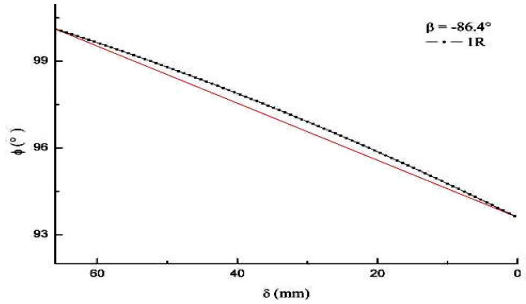

(a) Section 1R

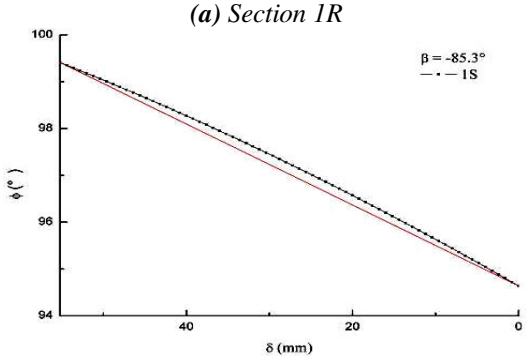

(b) Section 1S

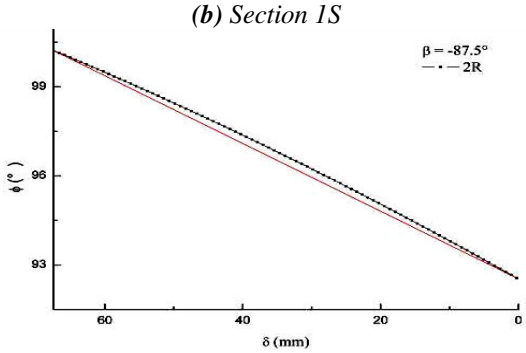

(c) Section 2R

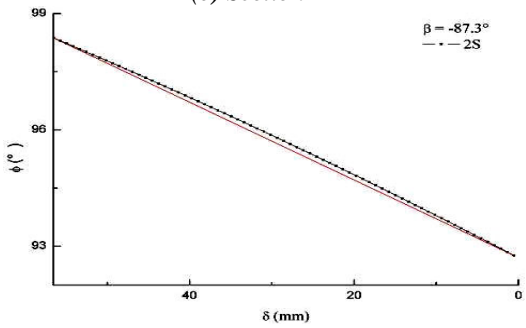

(d) Section 2S

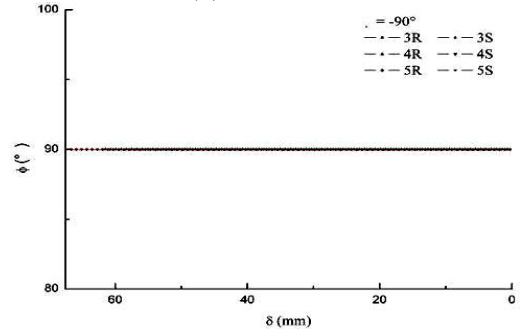

(e) Section 3, 4, 5

Figure 8: *Relationship of direction angle of the neutral axis vs. half of the width of the steel elastic zone*

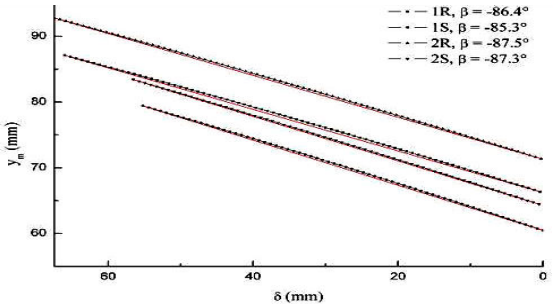

(a) Section 1, 2

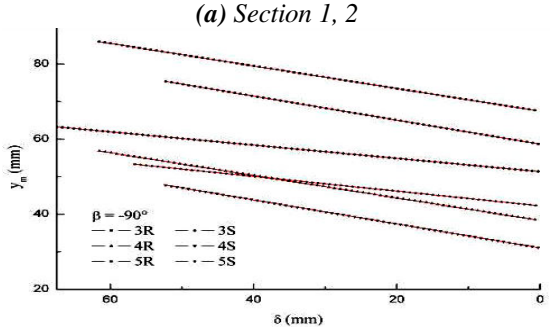

(b) Section 3, 4, 5

Figure 9: *Relationship of y coordinate of point m on the neutral axis vs. half of the width of the steel elastic zone*

3.4 Comparison of Bearing Capacity:

The relationship of bending moment vs. half of the width of the steel elastic zone of each specimen is shown in Figure 10. When half of the width of the steel elastic zone reduces to zero, the bending moment will reach its ultimate bending moment (seen from Figure 10). Based on Table 2 and Figure 10, it can be concluded that section 3R has the best carrying capacity and section 5S has the worst carrying capacity. Compared with the bearing capacity of section 5S which is a square cross section with uniform wall thickness, the bearing capacity of section 1R, 1S, 2R, 2S, 3R, 3S, 4R, 4S and 5R increases by 24.8%, 11.2%, 21.8%, 8.3%, 40.4%, 21.6%, 28.7%, 10.3% and 13.1% respectively. Based on Figures 6 and 7, it can be seen that the bearing capacity of the rectangular cross section of each section type is superior to the corresponding square cross section, which is because that in the case of a certain steel ratio more material lying away from the neutral axis will lead to better bearing capacity.

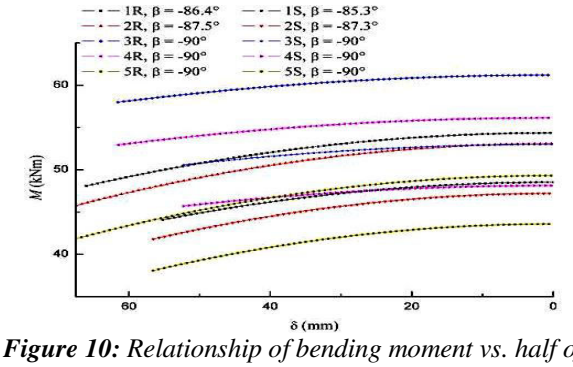

Figure 10: *Relationship of bending moment vs. half of the width of the steel elastic zone*

4. Conclusion:

In this paper, asymmetric rectangular CFST beams with unequal wall thickness subjected to pure bending in the elastic plastic stage are focused on. The case study of ten CFST beams with different cross sections is carried out. The following results of the study are worth noting:

(1) For an asymmetric cross section, the neutral axis in the elastic plastic stage will move and rotate nonlinearly with the plastic development of the cross section, and the translation and rotation of the neutral axis will undergo a fast-slow-fast process.

(2) For a symmetric cross section, the neutral axis in the elastic plastic stage will only move linearly with the plastic development of the cross section, and never rotate.

(3) When the ultimate bending moment is collinear with the neutral axis, the ultimate bending moment will reach its maximum.

(4) When the amount of material is fixed, the bearing capacity of a CFST beam can be significantly improved by the reasonable arrangement of the cross section.

Acknowledgements:

The financial support from the National Natural Science Foundation of China (numbers 51278298 and 50978162) is gratefully appreciated.

References

[1] L.H. Guo, Y.Y. Wang and S.M. Zhang, "Experimental study of concrete-filled rectangular HSS columns subjected to biaxial bending", *Advances in Structural Engineering*, 15, 1329-1344, 2012.

[2] L.H. Han, "Tests on stub columns of concrete-filled rhs sections", *Journal of Constructional Steel Research*, 58, 353-372, 2002.

[3] H. Zhang, "Thermodynamic property of concrete and temperature field analysis of the base plate of intake tower during construction period", *International Journal of Heat and Technology*, 33, 1, 145-154, 2015.

[4] C.Z. Xiao, S.H. Cai, T. Chen and C.L. Xu, "Experimental study on shear capacity of circular concrete filled steel tubes", *Steel and Composite Structures*, 13, 437-449, 2012.

[5] J.P. Liu, X.D. Wang, H.T. Qi and S.M. Zhang, "Behavior and strength of circular tubed steel-reinforced-concrete short columns under eccentric loading", *Advances in Structural Engineering*, 18, 1587-1595, 2015.

[6] J. Song and F.Y. Chen, "Calculation model for thermo-mechanical coupling and 3D numerical simulation for concrete tower of cable-stayed bridge", *International Journal of Heat and Technology*, 2, 1, 9-12, 2015.

[7] K.S. Chung, J.H. Kim and J.H. Yoo, "Experimental and analytical investigation of high-strength concrete-filled steel tube square columns subjected to flexural loading", *Steel and Composite Structures*, 14, 133-153, 2013.

[8] Dai X. and Lam D., "Axial compressive behaviour of stub concrete-filled columns with elliptical stainless steel hollow sections", *Steel and Composite Structures*, 10, 517-539, 2010.

[9] Giakoumelis G. and Lam D., "Axial capacity of circular concrete-filled tube columns", *Journal of Constructional Steel Research*, 60, 1049-1068, 2004.

[10] Gupta P.K., Sarda S.M. and Kumar M.S., "Experimental and computational study of concrete filled steel tubular columns under axial loads", *Journal of Constructional Steel Research*, 63, 182-193, 2007.

[11] Kvedaras A.K., Sauciuvenas G., Komka A. and Jarmolajeva E., "Analysis of behaviour for hollow/solid concrete-filled chs steel beams", *Steel and Composite Structures*, 19, 293-308, 2015.

[12] F.W. Lu, S.P. Li, D.W. Li and G.J. Sun, "Flexural behavior of concrete filled non-uni-thickness walled rectangular steel tube", *Journal of Constructional Steel Research*, 63, 1051-1057, 2007.